Identifying Practical DFT Functional for Predicting 0D and 1D Organic Metal Halide Hybrids

Yufang He[1], Md Sazedul Islam[1], Jarek Viera[1], Hanwei Gao[2], Jianwei Sun[3], Biwu Ma[1,*], and Bin Ouyang[1,*]

[1]Department of Chemistry and Biochemistry, Florida State University, Tallahassee, FL 32304

[2]Department of Physics, Florida State University, Tallahassee, FL, 32304

[3]Department of Physics and Engineering Physics, Tulane University, New Orleans, LA 70118

*Email: bma@fsu.edu; bouyang@fsu.edu

Abstract

Low dimensional organic metal halide hybrids (LD-OMHHs) have recently emerged as a new class of functional materials with various potential applications in optical, magnetic, and quantum information technologies. The high-throughput discovery and understanding of these materials necessitate identifying the best theoretical methods for generating reliable predictions of properties compared to experimental results. One of the key properties that has been studied is the band gap. This work systematically benchmarks several widely used density functional theory (DFT) functionals as well as the impact of spin-orbit coupling on band gap predictions for 115 experimentally reported LD-OMHHs. Surprisingly, it was found that the band gap predicted by GGA aligns similarly or better with experimentally measured values compared with two meta-GGA methods. Moreover, the inclusion of spin-orbital coupling has limited influence on band gap prediction. Such behavior can be understood by the potential existence of large excitonic effects in LD-OMHHs, which deviate computed fundamental gap from high-level DFT theory from experimental optical bandgap. Our research also reveals that the utilization of GGA functional without spin orbital coupling can be a practical and efficient method for the high-throughput screening of LD-OMMHs with reasonable band gaps.

1. Introduction

Low dimensional organic metal halide hybrids (LD-OMHHs) [1-4] have recently been developed as versatile material platforms with applications in various types of optoelectronic devices, such as photovoltaic cells (PVs), light emitting diodes (LEDs), and photodetectors for their unique and remarkable optical and electronic properties [5-8] . Unlike conventional perovskite structure with metal halide polyhedral connecting to form 3D frameworks, LD-OMHHs contain anionic metal halide species isolated and surrounded by organic cations, forming 2D, 1D, and 0D structures at the molecular level [9, 10]. Due to the site isolation and quantum confinement effects, LD OMHHs exhibit distinct properties as compared to their 3D perovskites. For instance, the corrugated-2D and 1D OMHHs with electronic band formation and structural distortions exhibit broadband emissions from a combination of direct and self-trapped excited states, producing near-white emissions[4, 11, 12] . 0D OMHHs without electronic band formation show broadband emissions from the reorganized excited states, with high photoluminescence quantum efficiencies (PLQEs) of up to 100 %)[3, 13-16].

Accurate prediction of properties of such organometallic halides urges systematic benchmark towards experimental results. Among all these applications, one common task for theoretical computation is to predict the band structure and band gap. However, which DFT functional is optimal for exploring and predicting the bandgap of LD-OMHH systems remains uncertain. In this work, we have conducted a systematic evaluation of the prediction power of different DFT functionals in terms of band gap prediction for LD-OMHHs, in particular 0D and 1D ones. The experimental band gap of 61 0D-OMHH and 54 1D-OMHHs are extracted from literatures to serve as the "ground truth" of our prediction. Four types of DFT setup, GGA, GGA with spin-orbital coupling (denoted as GGA+SOC), R2SCAN, and TASK are benchmarked on the 115 OMHHs. Specifically, R2SCAN is shown as low scaling

metaGGA method[17] that is able to offer accurate prediction of both formation enthalpy and band gaps[18-21]. On the other hand, TASK has emerged as a meta-GGA method that has lower computing cost than hybrid functionals but offers similar performance in terms of predicting bandgaps for perovskite and perovskite-related materials [22, 23]. Surprisingly, we have found out that the GGA level of theory outperforms TASK and gets very close to R2SCAN in terms of predicting band gap for 0D and 1D OMHHs. Given that it is well known in the field of DFT that semi-local methods such as GGA will always underestimate the bandgap [22, 24, 25] , our unexpected observations reveal there could be unprecedented excitonic effects in such systems, which makes the DFT predicted fundamental gap differs a lot from the optical band gap. Nevertheless, our analysis indicates that GGA by itself will be useful to massively screen down OMHHs with proper optical band gap, while the more physically insightful investigation may be subjected to investigating the shortlist of materials by combining hyper GGA level of theory or beyond with experimental measurement of excitonic effect [25].

2. Methodology

To investigate the electronic property of 0D and 1D OMHHs, density functional theory (DFT) calculations were carried out using the Vienna Ab Initio Simulation Package[26] and the projector-augmented wave (PAW) method [27, 28]. A reciprocal mesh discretization of 25 $Å^{-1}$ has been used for each calculation. Both lattice parameters and atomic positions were relaxed in DFT calculations. The convergence criteria were set as 10^{-6} eV for electronic iterations and 0.05 eV/Å for ionic iterations. Such convergence criterion has been tested to give neglectable energy difference compared with much more strict accuracy setup. A Gaussian type smearing of Fermi level was applied. A plane wave energy cutoff of 520 eV was used for all calculations. All structural optimizations are done with GGA before applying different methods for band structure calculations.

Many 0D and 1D OMHHs have large unit cell of more than 100 atoms, in some cases larger than 500 atoms. It is possible to calculate a few band structures with higher level theory, such as hybrid functionals, GW, random phase approximation and Quantum Monte Carlo [29-34] etc. However, given the extremely high cost to do high throughput screening with such functionals, we regard the use of hyper-GGA or higher-level theory as impractical for large scale screening of OMHHs.

3. Results

3.1. Coverage of chemical spaces of OMHHs

The compositional space of our examined compounds is demonstrated in Fig. 1. Particularly, 61 0D OMHHs and 54 1D OMHHs are obtained from existing literatures. Representative 0D and 1D OMHHs are demonstrated in Fig. 1(a), 1(d) respectively. The coverage of chemical spaces can be demonstrated by the histogram shown in Fig. 1. Additionally, these compounds are grouped depending on the metal species as well as number of carbon atom each organic molecule has (denoted as N_c per molecule in Fig. 1(c) and 1(f)). It can be inferred from Fig. 1(b) and Fig. 1(e) that the 0D OMHHs reported experimentally with band gap measurement are more diverse in metals, while around 49.18% 1D OMHHs are Pb contained compounds, in contrast to only 3.70% Pb containing compounds in the case of 0D OMHHs. Moreover, it can also be inferred from Fig. 1(c) and Fig. 1(f) that 0D OMHHs in general accommodate larger molecules with more carbon, this can be represented by compounds that have more than 20 C atom per molecule for 0D OMHHs as shown in Fig. 1(c), which is absent for 1D cases shown by Fig. 1(f). Some of the representative compounds with large organic molecules can be represented by $(C_{38}H_{34}P_2)MnBr_4$ with $(C_{38}H_{34}P_2)^+$ as the organic cation [35], $C_{24}H_{20}PCuBr_2$ with $(C_{24}H_{20}P)^+$ as organic cation as well as $C_{24}H_{20}P_2ZnBr_4$ with $(C_{24}H_{20}P_2)^{2+}$ as organic cation. Such

distribution of molecular size can be understood as the fact that there is much less topological constraint for 0D OMHHs as the metal halide polyhedron does not need to connect in a way to maintain periodicity of the inorganic motif in any dimension.

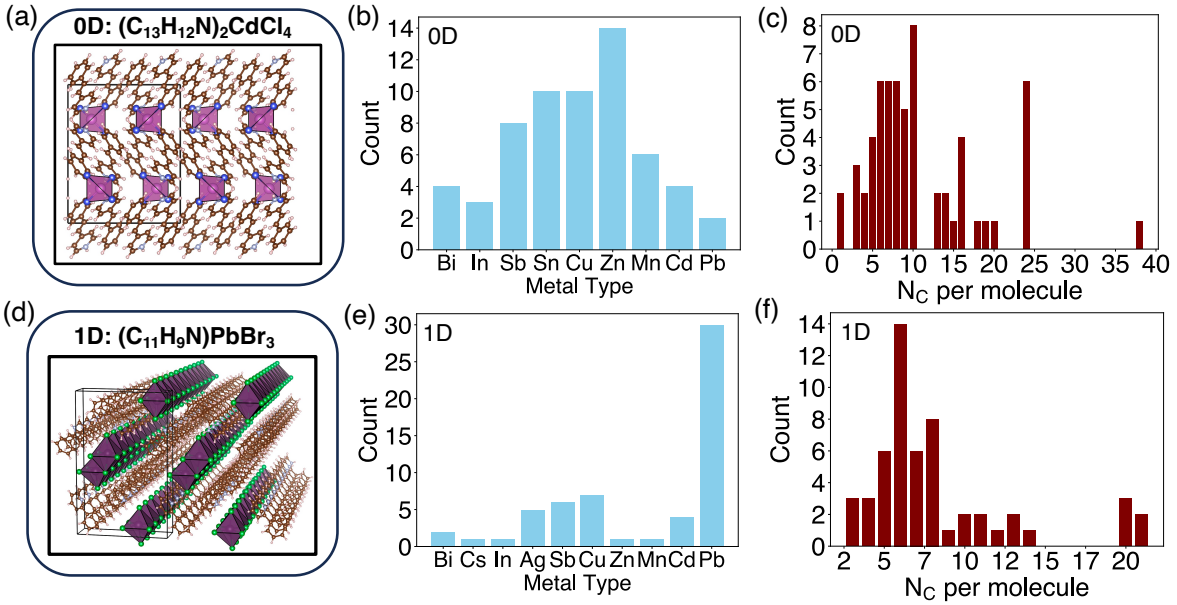

Fig. 1: Chemical spaces of examined 0D and 1D OMHHs: (a) crystal structure of representative 0D OMHHs-$(C_{13}H_{12}N)_2CdCl_4$; (b) metal species and (c) number of carbon atoms each organic molecule (denoted as N_c per molecule) of 0D OMHHs; (d) crystal structure of representative 1D OMHHs-$(C_{11}H_9N)PbBr_3$; (e) metal species and (f) N_c per molecule of 1D OMHHs.

3.2. Comparison among GGA, R2SCAN, and TASK

With the establishment of all datasets, we then computed the band structure using three types of functionals: GGA, R2SCAN, and TASK. GGA is the most widely used functional and offers a reasonable estimation of material properties in many situations [36]. On the other hand, R2SCAN[17, 37, 38] emerges recently as a low scaling metaGGA method that offered improved accuracy for many properties, such as formation enthalpy, decomposition energy as well as mechanical properties etc. Last but not least, TASK is also selected for comparison as it was recently reported to be functional and capable of predicting bandgap with similar behavior to the HSE level of hybrid functionals but with much less cost [22]. It is also reported

that TASK offers a better prediction of the bandgap of halide perovskites, which is a chemical system close to the material systems discussed in this work.

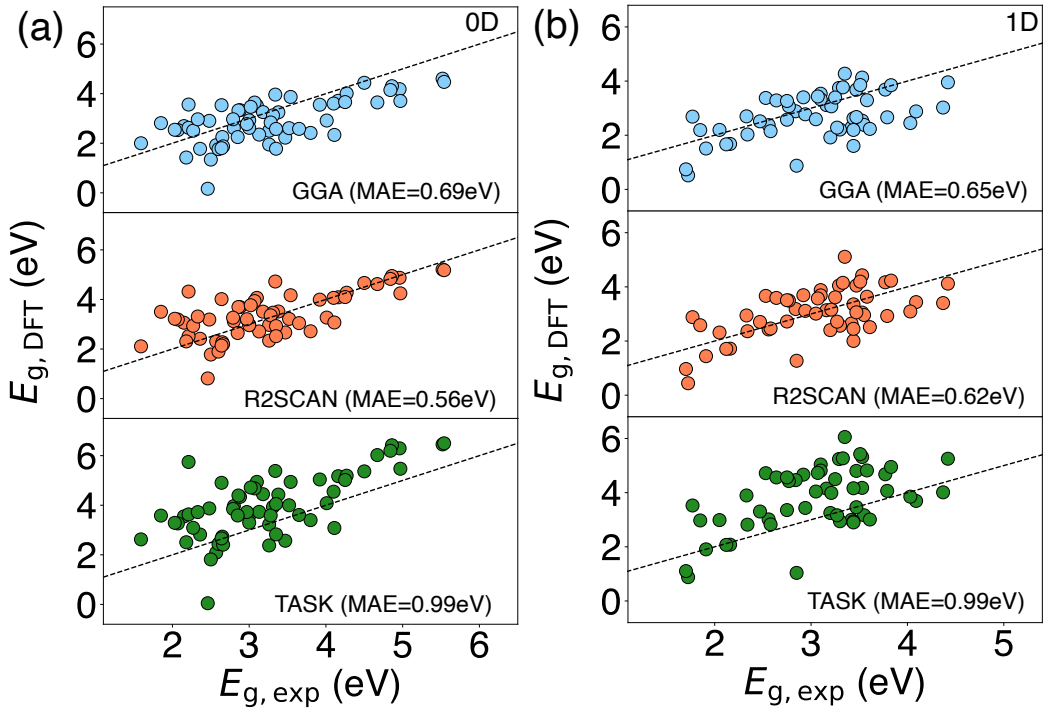

Fig. 2: Comparison of band gap estimation of (a) 0D and (b) 1D OMHHs from GGA, R2SCAN, and TASK with experimental band gap reported in literatures.

The parity plot of experimental band gap versus DFT computed ones using different functionals are demonstrated in Fig. 2. Here we separate 0D compounds with 1D compounds to check whether the dimensionality of metal-halide bond topology will play a role in the prediction accuracy. Several interesting observations can be made from Fig. 2. Particularly, R2SCAN tends out to show the best prediction accuracy among three functionals, for both 0D and 1D materials. However, the mean absolute error (MAE) predictions from R2SCAN are quite close to GGA, with slight difference of 0.14 eV for the 0D case versus 0.03 eV for the 1D case. On the other hand, TASK tends to mostly overestimate the band gap with the MAE values being 0.99 eV for both cases, which is 0.30 eV and 0.34 eV larger than the GGA prediction. The observation for band gap prediction from TASK is also consistent with the

fact that the HSE level of theory can be liable to predict band gap than GGA level of theory [39-42], particularly considering that TASK is claimed to be able to match HSE band structure prediction with much lower computing cost [22]. Additionally, one other trend that can be inferred from Fig. 2 is that both R2SCAN and TASK tend to predict larger band gap values than GGA in general. This is also consistent with the typical understanding that GGA tends to underestimate band gaps compared with other DFT methods[17, 24, 37, 43, 44].

3.3. The impact of spin orbital coupling

Another important setup for band structure calculations is whether to consider the relativistic effect through spin orbital coupling. This can be a relevant effect especially considering that many OMHHs involve heavy metals such as Pb, Bi, Sn etc. The comparison between GGA predicted band gap and band gaps predicted by GGA plus spin orbital coupling (denoted as GGA+SOC) are presented in Fig. 3. Both 0D and 1D predictions are combined in this plot given that we did not find any significantly different trends across different dimensionalities. It can be inferred from Fig. 3(a) that the general performance between GGA and GGA+SOC are similar. There is no obvious improvement given that both MAEs are 0.67 eV when calculated from all 0D and 1D OMHHs. Moreover, another interesting observation can be illustrated by Fig. 3(b). It can be inferred that almost all GGA+SOC prediction yields smaller band gap than GGA by itself. However, this systematic shift of predictions does not necessarily help or hurt the prediction error as it helps the cases when GGA overestimate the band gap, but it will make things worse when GGA underestimate the experimental gaps. To illustrate such a "double-edged sword" effect brought by incorporating SOC, we have demonstrated one case when the underestimation brought by SOC deviate further away from experimental gap (GGA: 3.29 eV, GGA+SOC 2.86 eV, experiment: 3.58 eV) as shown by the calculations of $(C_4H_{14}N_2)PbCl_4$ in Fig. 3(c),

as well as one case when the lowering of band gap of $(C_7H_{13}N_2)PbCl_3$ brought by SOC helps get close to the experimental values (GGA: 4.13 eV, GGA+SOC 3.56 eV, experiment: 3.53 eV).

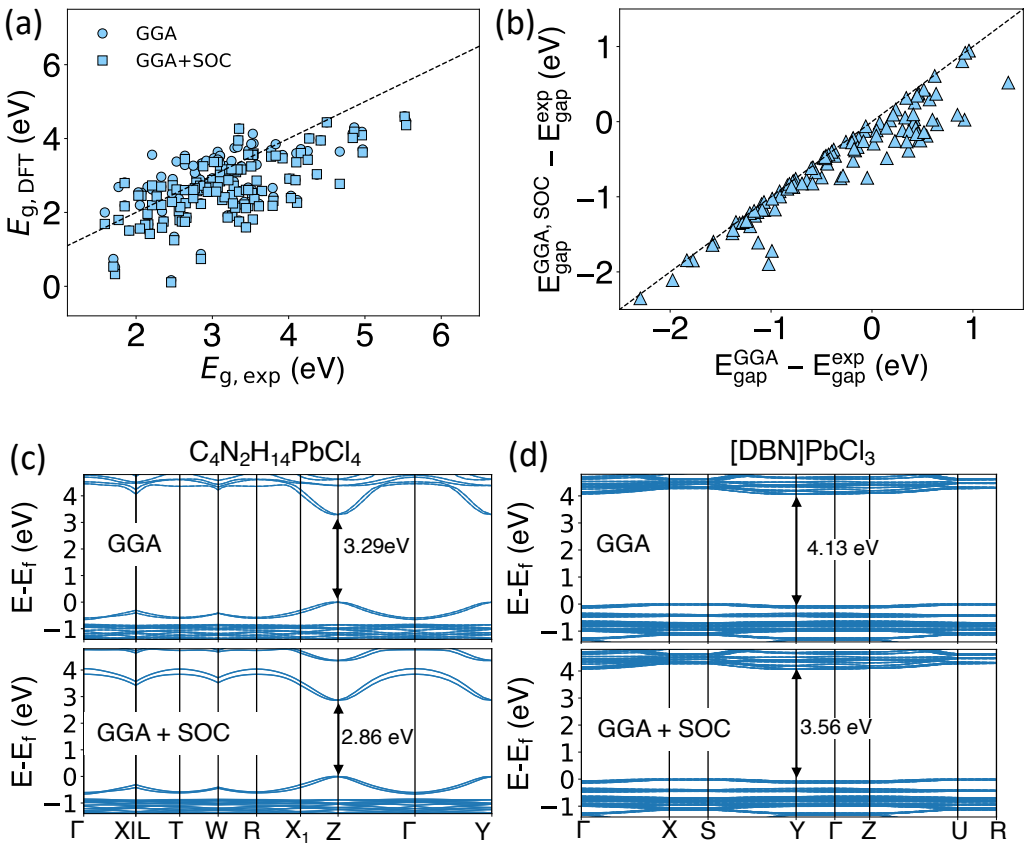

Fig. 3: (a) The comparison between GGA predicted band gap and band gaps predicted by GGA plus spin orbital coupling (denoted as GGA+SOC); (b) the band gap difference of GGA vs experiment versus the band gap difference of GGA+SOC vs experiment; (c) the band structure of representative compounds of $(C_4H_{14}N_2)PbCl_4$ with better GGA estimation of band gap; (d) the band structure of representative compounds of $(C_7H_{13}N_2)PbCl_3$ with better GGA+SOC estimation of band gap. For (c) and (d), the direct gap used to compare with optical measurement is illustrated by black arrows.

4. Discussions

4.1. Statistical trends of prediction errors

Based on the performance analysis of different DFT functionals. We end up with a very interesting observation --- GGA turns out to be a suitable choice for predicting band gap compared with GGA+SOC and two metaGGA functionals. In this section, we want to

demonstrate a bit more interpretations of the behavior of different functionals as well as provide more insights into the usage of different functionals for high throughput screening of electronic structures of OMHHs.

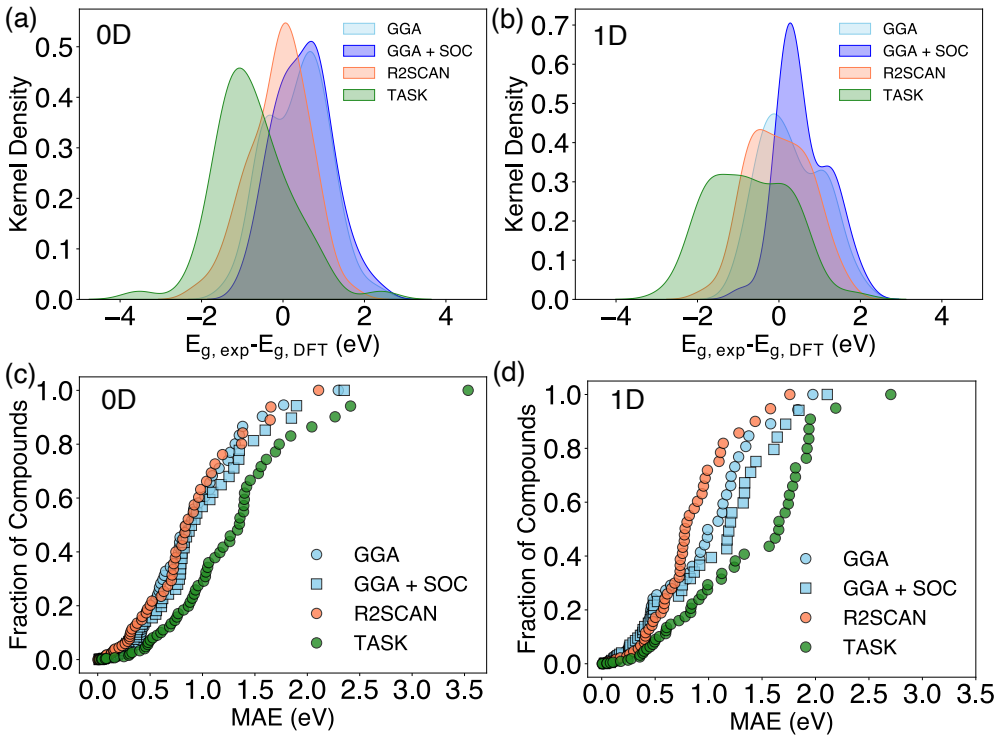

Fig. 4: The Kernel density distributions of (a) 0D and (b) 1D OMHHs from GGA, GGA+SOC, R2SCAN, and TASK; The fraction of compounds vs MAE of (c) 0D and (d) 1D OMHHs from GGA, GGA+SOC, R2SCAN, and TASK.

The distributions and statistical features of predictions errors are demonstrated in Fig. 4. Particularly, the kernel density distribution of all four DFT setups for 0D and 1D OMHHs are demonstrated in Fig. 4(a) and Fig. 4(b) respectively. Such distributions will further clarify the fact that in general the band gap values predicted by different values follow the order GGA+SOC ≈ GGA < R2SCAN < TASK, which can be roughly estimated by peak position. Moreover, the fact that the kernel distribution of TASK prediction error centers at ~ 1.5 eV indicates that TASK in general tends to overestimate experimental band gap by such value. On the other hand, the distribution of other three DFT setups will center around 0 eV,

indicating much less systematic errors. Moreover, another way of systematically look at the prediction performance is to plot the fraction of data for specific MAE value, which are demonstrated in Fig. 4(c) and 4(d). It can be seen from these two figures that half of the dataset for both 0D and 1D can be accurately predicted with MAE smaller than 0.7 eV using GGA, GGA+SOC or R2SCAN, which will still be useful for estimating optical performance as well as electronic conductivity of such materials. On the other hand, TASK tends to mis-predict the band gap of almost 80% of candidates with MAE more than 1eV. Moreover, even though R2SCAN shows slightly lower MAE for predicting the experimental band gaps, the difference is marginal as shown in Fig. 4(c) and Fig. 4(d), particularly in the case of predicting 0D OMHHs.

4.2. Strategy of choosing DFT setups for predicting bandgap

It seems that there is no perfect way of predicting bandgap of OMHHs. However, it is also obvious that it is not necessary to go to metaGGA level of theory to improve the accuracy of bandgap prediction for matching experimental measurements. Particularly, the computational cost for calculating band gaps using GGA+SOC, R2SCAN and TASK are demonstrated in Fig. 5. All three methods are shown in Fig. 5 to cost in general four times more computing resources than GGA. Given the fact that they did not provide obvious improvement of bandgap prediction accuracy. It is fair to suggest that GGA should be sufficient for performing high throughput screening of OMHHs for obtaining reasonable estimation of band structures. After the high throughput screening, a shortlist of candidates can then be collected for more accurate estimation using more advanced methods, such as hyperGGA level of theory, random phase approximation, GW, Quantum Monte Carlo etc.

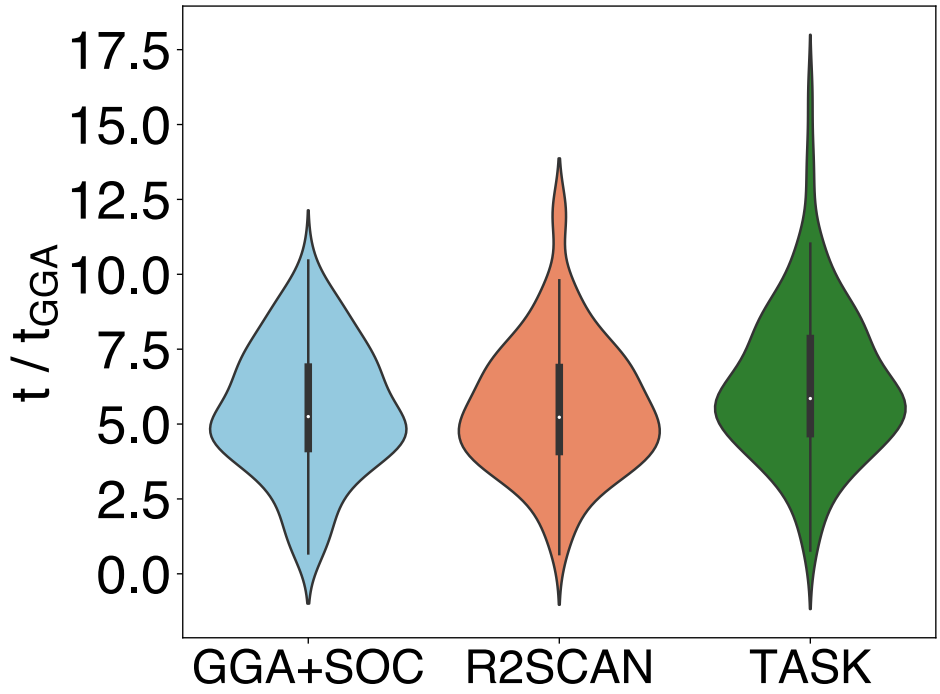

Fig. 5: The computational cost for calculating band gaps using GGA+SOC, R2SCAN and TASK compared with GGA.

4.3. Physical interpretation

In addition to prediction accuracy, another important aspect is why GGA does not show worse performance than other higher-level methods, e.g., GGA+SOC, R2SCAN, and TASK. This is counter-intuitive and against the common understanding that semi-local theory such as GGA is generally regarded to underestimate fundamental band gap[24]. A reasonable hypothesis to understand such behavior is that most of our examined material systems have strong excitonic effect, which make the DFT predicted fundamental band gap larger than optical band gap measured experimentally from physics. In this case, TASK may demonstrate the correct physics by overestimating the optical band gap as the DFT results only indicates the value of fundamental band gap. There is a possibility for this hypothesis, but it cannot be verified in the scope of this research due to the lack of data that demonstrates the excitonic effect in LD-OMHHs. A comprehensive combination between experimental

measurement and higher level DFT calculations may be beneficial to provide answer to this puzzle. However, regardless of the real reason for such trend, our results demonstrate that the optical band gap can be efficiently captured by GGA level of theory, even if it could be due to wrong reason. It underscores the effectiveness of using GGA calculations for prescreen of good OMHH materials for optoelectronic, electronic or quantum information application, which is a very useful discovery for high throughput materials screening.

5. Conclusion

In summary, we have presented a systematic evaluation of different DFT functionals, such as GGA, R2SCAN and TASK, as well as the inclusion of spin orbital coupling, in terms of band gap prediction for 0D and 1D OMHHs. The experimental band gap of 61 0D and 54 1D OMHHs are extracted from literatures to serve as the "ground truth" of different DFT functionals prediction. Unexpectedly, the accuracy of GGA calculation for OMHHs is comparable to R2SCAN or even better than TASK. Given that GGA offers a reasonable MAE for predicting all band gaps (e.g. ~0.6 eV), it can be used as a more practical method for accurately screen of electronic property of OMHHs systems.

Acknowledgement

Y. He, H. Gao and B. Ouyang want to acknowledge the support from the FSU CRC Seed Grant Program and the Startup funding for assistant professor. M. S. Islam, J. Viera and B. Ma want to acknowledge the funding support from the National Science Foundation (NSF) (DMR-2204466). The computational resources were provided by the Advanced Cyberinfrastructure Coordination Ecosystem: Services & Support (ACCESS), the National Energy Research Scientific Computing Center (NERSC), a DOE Office of Science User Facility supported by the Office of Science and the U.S. Department of Energy under contract no. DE-AC0205CH11231 and Research Computing Center (RCC) at Florida State University. The computation and data processing were also supported by the supercomputing resources from the Department of Energy's Office of Energy Efficiency and Renewable Energy at the National Renewable Energy Laboratory.

Conflict of Interest

The authors declare no competing interests.

References

1. Lin, H.; Zhou, C.; Tian, Y.; Siegrist, T.; Ma, B., Low-dimensional organometal halide perovskites. *ACS Energy Letters* **2017,** *3* (1), 54-62.
2. Zhou, C.; Lin, H.; Shi, H.; Tian, Y.; Pak, C.; Shatruk, M.; Zhou, Y.; Djurovich, P.; Du, M. H.; Ma, B., A zero-dimensional organic seesaw-shaped tin bromide with highly efficient strongly stokes-shifted deep-red emission. *Angewandte Chemie* **2018,** *130* (4), 1033-1036.
3. Zhou, C.; Tian, Y.; Wang, M.; Rose, A.; Besara, T.; Doyle, N. K.; Yuan, Z.; Wang, J. C.; Clark, R.; Hu, Y., Low-dimensional organic tin bromide perovskites and their photoinduced structural transformation. *Angewandte Chemie International Edition* **2017,** *56* (31), 9018-9022.
4. Yuan, Z.; Zhou, C.; Tian, Y.; Shu, Y.; Messier, J.; Wang, J. C.; Van De Burgt, L. J.; Kountouriotis, K.; Xin, Y.; Holt, E., One-dimensional organic lead halide perovskites with efficient bluish white-light emission. *Nature communications* **2017,** *8* (1), 14051.
5. Tan, Z.-K.; Moghaddam, R. S.; Lai, M. L.; Docampo, P.; Higler, R.; Deschler, F.; Price, M.; Sadhanala, A.; Pazos, L. M.; Credgington, D., Bright light-emitting diodes based on organometal halide perovskite. *Nature nanotechnology* **2014,** *9* (9), 687-692.
6. Kojima, A.; Teshima, K.; Shirai, Y.; Miyasaka, T., Organometal halide perovskites as visible-light sensitizers for photovoltaic cells. *Journal of the american chemical society* **2009,** *131* (17), 6050-6051.
7. Xing, G.; Mathews, N.; Lim, S. S.; Yantara, N.; Liu, X.; Sabba, D.; Grätzel, M.; Mhaisalkar, S.; Sum, T. C., Low-temperature solution-processed wavelength-tunable perovskites for lasing. *Nature materials* **2014,** *13* (5), 476-480.
8. Ling, Y.; Yuan, Z.; Tian, Y.; Wang, X.; Wang, J. C.; Xin, Y.; Hanson, K.; Ma, B.; Gao, H., Bright light-emitting diodes based on organometal halide perovskite nanoplatelets. *Advanced materials* **2016,** *28* (2), 305-311.
9. Worku, M.; Ben-Akacha, A.; Blessed Shonde, T.; Liu, H.; Ma, B., The past, present, and future of metal halide perovskite light-emitting diodes. *Small Science* **2021,** *1* (8), 2000072.
10. Zhou, C.; Lin, H.; He, Q.; Xu, L.; Worku, M.; Chaaban, M.; Lee, S.; Shi, X.; Du, M.-H.; Ma, B., Low dimensional metal halide perovskites and hybrids. *Materials Science and Engineering: R: Reports* **2019,** *137*, 38-65.
11. Lin, H.; Zhou, C.; Neu, J.; Zhou, Y.; Han, D.; Chen, S.; Worku, M.; Chaaban, M.; Lee, S.; Berkwits, E., Bulk assembly of corrugated 1D metal halides with broadband yellow emission. *Advanced Optical Materials* **2019,** *7* (6), 1801474.
12. Huang, J.; Peng, Y.; Jin, J.; Molokeev, M. S.; Yang, X.; Xia, Z., Unveiling white light emission of a one-dimensional Cu (I)-based organometallic halide toward single-phase light-emitting diode applications. *The Journal of Physical Chemistry Letters* **2021,** *12* (51), 12345-12351.
13. Zhou, C.; Lin, H.; Tian, Y.; Yuan, Z.; Clark, R.; Chen, B.; van de Burgt, L. J.; Wang, J. C.; Zhou, Y.; Hanson, K., Luminescent zero-dimensional organic metal halide hybrids with near-unity quantum efficiency. *Chemical science* **2018,** *9* (3), 586-593.

14. Zhou, C.; Lin, H.; Lee, S.; Chaaban, M.; Ma, B., Organic–inorganic metal halide hybrids beyond perovskites. *Materials Research Letters* **2018,** *6* (10), 552-569.
15. Huang, J.; Su, B.; Song, E.; Molokeev, M. S.; Xia, Z., Ultra-broad-band-excitable Cu (I)-based organometallic halide with near-unity emission for light-emitting diode applications. *Chemistry of Materials* **2021,** *33* (12), 4382-4389.
16. Zhou, C.; Xu, L. J.; Lee, S.; Lin, H.; Ma, B., Recent advances in luminescent zero-dimensional organic metal halide hybrids. *Advanced Optical Materials* **2021,** *9* (18), 2001766.
17. Kothakonda, M.; Kaplan, A. D.; Isaacs, E. B.; Bartel, C. J.; Furness, J. W.; Ning, J.; Wolverton, C.; Perdew, J. P.; Sun, J., Testing the r2SCAN Density Functional for the Thermodynamic Stability of Solids with and without a van der Waals Correction. *ACS Materials Au* **2022,** *3* (2), 102-111.
18. Medvedev, M. G.; Bushmarinov, I. S.; Sun, J.; Perdew, J. P.; Lyssenko, K. A., Density functional theory is straying from the path toward the exact functional. *Science* **2017,** *355* (6320), 49-52.
19. Peng, H.; Yang, Z.-H.; Perdew, J. P.; Sun, J., Versatile van der Waals density functional based on a meta-generalized gradient approximation. *Physical Review X* **2016,** *6* (4), 041005.
20. Zhang, Y.; Sun, J.; Perdew, J. P.; Wu, X., Comparative first-principles studies of prototypical ferroelectric materials by LDA, GGA, and SCAN meta-GGA. *Physical Review B* **2017,** *96* (3), 035143.
21. Zhang, Y.; Kitchaev, D. A.; Yang, J.; Chen, T.; Dacek, S. T.; Sarmiento-Pérez, R. A.; Marques, M. A. L.; Peng, H.; Ceder, G.; Perdew, J. P.; Sun, J., Efficient first-principles prediction of solid stability: Towards chemical accuracy. *npj Computational Materials* **2018,** *4* (1), 9.
22. Lebeda, T.; Aschebrock, T.; Sun, J.; Leppert, L.; Kümmel, S., Right band gaps for the right reason at low computational cost with a meta-GGA. *Physical Review Materials* **2023,** *7* (9), 093803.
23. Aschebrock, T.; Kümmel, S., Ultranonlocality and accurate band gaps from a meta-generalized gradient approximation. *Physical Review Research* **2019,** *1* (3), 033082.
24. Perdew, J. P.; Yang, W.; Burke, K.; Yang, Z.; Gross, E. K.; Scheffler, M.; Scuseria, G. E.; Henderson, T. M.; Zhang, I. Y.; Ruzsinszky, A., Understanding band gaps of solids in generalized Kohn–Sham theory. *Proceedings of the national academy of sciences* **2017,** *114* (11), 2801-2806.
25. Qiu, D. Y.; Da Jornada, F. H.; Louie, S. G., Optical spectrum of MoS 2: many-body effects and diversity of exciton states. *Physical review letters* **2013,** *111* (21), 216805.
26. Hafner, J.; Kresse, G., The vienna ab-initio simulation program VASP: An efficient and versatile tool for studying the structural, dynamic, and electronic properties of materials. In *Properties of Complex Inorganic Solids*, Springer: 1997; pp 69-82.
27. Perdew, J. P.; Burke, K.; Ernzerhof, M., Generalized gradient approximation made simple. *Physical review letters* **1996,** *77* (18), 3865.
28. Kresse, G.; Furthmüller, J., Efficient iterative schemes for ab initio total-energy calculations using a plane-wave basis set. *Physical review B* **1996,** *54* (16), 11169.

29. Śmiga, S.; Constantin, L. A., Unveiling the physics behind hybrid functionals. *The Journal of Physical Chemistry A* **2020,** *124* (27), 5606-5614.
30. Arbuznikov, A., Hybrid exchange correlation functionals and potentials: Concept elaboration. *Journal of Structural Chemistry* **2007,** *48*, S1-S31.
31. Paier, J.; Janesko, B. G.; Henderson, T. M.; Scuseria, G. E.; Grüneis, A.; Kresse, G., Hybrid functionals including random phase approximation correlation and second-order screened exchange. *The Journal of chemical physics* **2010,** *132* (9).
32. Ceperley, D.; Alder, B., Quantum monte carlo. *Science* **1986,** *231* (4738), 555-560.
33. Co', G., Introducing the random phase approximation theory. *Universe* **2023,** *9* (3), 141.
34. Gerosa, M.; Bottani, C.; Di Valentin, C.; Onida, G.; Pacchioni, G., Accuracy of dielectric-dependent hybrid functionals in the prediction of optoelectronic properties of metal oxide semiconductors: a comprehensive comparison with many-body GW and experiments. *Journal of Physics: Condensed Matter* **2018,** *30* (4), 044003.
35. Xu, L.-J.; Lin, X.; He, Q.; Worku, M.; Ma, B., Highly efficient eco-friendly X-ray scintillators based on an organic manganese halide. *Nature communications* **2020,** *11* (1), 4329.
36. Jain, A.; Ong, S. P.; Hautier, G.; Chen, W.; Richards, W. D.; Dacek, S.; Cholia, S.; Gunter, D.; Skinner, D.; Ceder, G., Commentary: The Materials Project: A materials genome approach to accelerating materials innovation. *APL materials* **2013,** *1* (1).
37. Sun, J.; Remsing, R. C.; Zhang, Y.; Sun, Z.; Ruzsinszky, A.; Peng, H.; Yang, Z.; Paul, A.; Waghmare, U.; Wu, X., Accurate first-principles structures and energies of diversely bonded systems from an efficient density functional. *Nature chemistry* **2016,** *8* (9), 831-836.
38. Liu, H.; Bai, X.; Ning, J.; Hou, Y.; Song, Z.; Ramasamy, A.; Zhang, R.; Li, Y.; Sun, J.; Xiao, B., Assessing r2SCAN meta-GGA functional for structural parameters, cohesive energy, mechanical modulus, and thermophysical properties of 3d, 4d, and 5d transition metals. *The Journal of Chemical Physics* **2024,** *160* (2).
39. Henderson, T. M.; Paier, J.; Scuseria, G. E., Accurate treatment of solids with the HSE screened hybrid. *physica status solidi (b)* **2011,** *248* (4), 767-774.
40. Vines, F.; Lamiel‐García, O.; Chul Ko, K.; Yong Lee, J.; Illas, F., Systematic study of the effect of HSE functional internal parameters on the electronic structure and band gap of a representative set of metal oxides. *Journal of computational chemistry* **2017,** *38* (11), 781-789.
41. Lucero, M. J.; Henderson, T. M.; Scuseria, G. E., Improved semiconductor lattice parameters and band gaps from a middle-range screened hybrid exchange functional. *Journal of Physics: Condensed Matter* **2012,** *24* (14), 145504.
42. Henderson, T. M.; Izmaylov, A. F.; Scuseria, G. E.; Savin, A., Assessment of a middle-range hybrid functional. *Journal of chemical theory and computation* **2008,** *4* (8), 1254-1262.
43. Yang, Z.-h.; Peng, H.; Sun, J.; Perdew, J. P., More realistic band gaps from meta-generalized gradient approximations: Only in a generalized Kohn-Sham scheme. *Physical review B* **2016,** *93* (20), 205205.

44. Borlido, P.; Schmidt, J.; Huran, A. W.; Tran, F.; Marques, M. A.; Botti, S., Exchange-correlation functionals for band gaps of solids: benchmark, reparametrization and machine learning. *npj Computational Materials* **2020,** *6* (1), 1-17.

Supplementary information

Identifying Practical DFT Functional for Predicting 0D and 1D Organic Metal Halide Hybrids

Yufang He[1], Md Sazedul Islam[1], Jarek Viera[1], Jianwei Sun[2], Biwu Ma[1,*], and Bin Ouyang[1,*]

[1]Department of Chemistry and Biochemistry, Florida State University, Tallahassee, FL 32304

[2]Department of Physics and Engineering Physics, Tulane University, New Orleans, LA 70118

*Email: bma@fsu.edu; bouyang@fsu.edu

Table S1. The band gap of experimental, GGA, GGA+SOC, R2SCAN, and TASK for 0D OMHHs.

Conventional name	Chemical formula	E_{Exp} (eV)	E_{GGA} (eV)	E_{GGA}^{SOC} (eV)	E_{R2SCAN} (eV)	E_{TASK} (eV)
$C_{16}H_{38}N_2MnBr_4$	$C_{16}H_{38}N_2MnBr_4$	4.67[1]	3.65	2.77	4.62	6.02
PPh_4CuBr_2	$C_{24}H_{20}PCuBr_2$	2.57[2]	1.92	1.79	2.31	2.09
$(PBA)_2ZnCl_4$	$(C_{10}H_{16}N)_2ZnCl_4$	4.50[3]	4.44	4.44	4.67	5.37
$(PBA)_2ZnI_4$	$(C_{10}H_{16}N)_2ZnI_4$	4.25[3]	3.66	3.43	4.10	5.02
$(Bmpip)_2Cu_2Br_4$	$(C_{10}H_{22}N)_2Cu_2Br_4$	3.13[2]	2.35	2.34	2.71	3.73
$(Bmpip)_2PbBr_4$	$(C_{10}H_{22}N)_2PbBr_4$	3.10[4]	3.51	3.13	4.06	4.94
$(Bmpip)_2ZnBr4$	$(C_{10}H_{22}N)_2ZnBr_4$	5.54[5]	4.47	4.36	5.18	6.50
$(C_{10}H_{28}N_4Cl_2)SnCl_4 \cdot 2H_2O$	$(C_{10}H_{28}N_4Cl_2)SnCl_4 \cdot 2H_2O$	4.16[6]	3.71	3.61	4.09	5.17
$(C_{10}H_{28}N_4)SnBr_6 \cdot 4H_2O$	$(C_{10}H_{28}N_4)SnBr_6 \cdot 4H_2O$	3.38[6]	3.25	3.16	3.51	4.43
$(C_{10}H_{28}N_4)SnI_6 \cdot 4H_2O$	$(C_{10}H_{28}N_4)SnI_6 \cdot 4H_2O$	3.18[6]	3.26	3.16	3.51	4.44
$(C_{13}H_{12}N)CdCl_4$	$(C_{13}H_{12}N)CdCl_4$	2.65[7]	2.25	2.25	2.27	2.73
$(1,3\text{-}dppH_2)_2Cu_4I_8 \cdot H_2O$	$(C_{13}H_{16}N_2)_2Cu_4I_8 \cdot H_2O$	2.46[8]	0.16	0.11	0.81	0.05
$(H_2TTz) \cdot ZnBr_4 \cdot MeOH$	$(C_{14}H_{10}N_4S_2)ZnBr_4 \cdot MeOH$	2.50[9]	1.34	1.25	1.78	1.81
$(H_2TTz)ZnCl_4 \cdot MeOH$	$(C_{14}H_{10}N_4S_2)ZnCl_4 \cdot MeOH$	2.66[9]	1.87	1.86	2.20	2.41
$(DTA)_2Cu_2I_4$	$(C_{15}H_{34}N)_2Cu_2I_4$	3.52[10]	2.61	2.52	3.21	4.00
$(C_{16}H_{28}N)_2SbCl_5$	$(C_{16}H_{28}N)_2SbCl_5$	3.31[11]	3.12	3.09	3.46	3.93
$(TBA)CuBr_2$	$(C_{16}H_{36}N)CuBr_2$	3.92[12]	3.55	3.46	3.99	5.04
$(TBA)CuI_2$	$(C_{16}H_{36}N)CuI_2$	3.35[13]	2.58	2.56	2.93	4.05
$(PPh_3H)_2SbCl_5$	$(C_{18}H_{16}P)_2SbCl_5$	3.00[14]	2.62	2.63	2.96	3.30
$(MTP)_2SbBr_5$	$(C_{19}H_{18}P)_2SbBr_5$	2.27[15]	2.51	2.43	2.94	3.09

$(ETP)_2MnBr_4$	$(C_{20}H_{20}P)_2MnBr_4$	3.35[16]	1.78	1.75	2.52	2.82
$(Ph_4P)Cd_2Br_6$	$(C_{24}H_{20}P)_2Cd_2Br_6$	3.28[17]	2.84	2.72	3.36	3.59
TPP_2MnCl_4	$(C_{24}H_{20}P)_2MnCl_4$	2.18[18]	1.42	1.42	2.31	2.51
TPP_2ZnBr_4	$(C_{24}H_{20}P)_2ZnBr_4$	2.03[18]	2.54	2.45	3.22	3.29
$TPP_2ZnCl_2Br_2$	$(C_{24}H_{20}P)_2ZnCl_2Br_2$	2.07[18]	2.53	2.45	3.19	3.27
TPP_2ZnCl_4	$(C_{24}H_{20}P)_2ZnCl_4$	1.85[18]	2.81	2.79	3.50	3.58
$(C_{38}H_{34}P_2)MnBr_4$	$(C_{38}H_{34}P_2)MnBr_4$	2.36[19]	1.77	1.75	2.41	2.82
$(C_3H_{12}N_2)_2Sb_2Cl_{10}$	$(C_3H_{12}N_2)_2Sb_2Cl_{10}$	3.80[20]	2.42	2.31	2.72	3.40
$(BPA)_2SnBr_6$	$(C_3H_9BrN)_2SnBr_6$	2.64[21]	1.80	1.75	2.14	2.66
$(BPA)_2SnCl_6$	$(C_3H_9BrN)_2SnCl_6$	2.97[21]	2.77	2.69	3.20	3.73
$(C_4N_2H_{14}Br)_4SnBr_6$	$(C_4N_2H_{14}Br)_4SnBr_6$	3.02[22]	3.47	3.37	3.77	4.72
$(C_4N_2H_{14}Br)_4SnI_6$	$(C_4N_2H_{14}Br)_4SnI_6$	2.48[22]	2.90	2.73	3.19	3.87
$(1\text{-}mPQBr)_2MnBr_4$	$(C_5H_{14}N_2Br)_2MnBr_4$	2.21[23]	3.56	2.73	4.32	5.74
$(H_2MPz)ZnBr_4$	$(C_5H_{14}N_2)ZnBr_4$	4.86[24]	4.30	4.18	4.94	6.42
$(H_2NMPz)ZnBr_4{\cdot}H_2O$	$(C_5H_{14}N_2)ZnBr_4{\cdot}H_2O$	4.96[24]	4.18	4.09	4.87	6.29
$(DPA)_2BiI_9$	$(C_5H_{16}N_2)_2BiI_9$	1.59[25]	2.00	1.69	2.10	2.62
$(Emim)_4Cu_4I_8$	$(C_6H_{11}N_2)_4Cu_4I_8$	3.26[26]	1.95	1.91	2.34	2.38
$(H_2AMP)CdBr_4{\cdot}H_2O$	$(C_6H_{15}N_2)CdBr_4{\cdot}H_2O$	4.97[27]	3.70	3.62	4.25	5.47
$(H_2AMPd)ZnBr_4{\cdot}H_2O$	$(C_6H_{16}N_2)ZnBr_4{\cdot}H_2O$	4.84[24]	4.15	4.02	4.83	6.20
$(DPA)_3SbCl_6$	$(C_6H_{16}N)_3SbCl_6$	3.07[28]	3.64	3.37	3.93	4.68
$(4cmpyH)_2BiCl_5$	$(C_6H_7ClN)_2BiCl_5$	3.26[29]	2.51	2.47	2.97	3.22
$(C_6H_9N_2)_2MnI_4$	$(C_6H_9N_2)_2MnI_4$	2.21[30]	2.62	2.20	2.51	3.63
$(N\text{-}EPD)_2ZnBr_4$	$(C_7H_{10}N)_2ZnBr_4$	4.11[31]	2.34	2.26	3.07	3.08
$(PMA)_2ZnI_4{\cdot}H_2O$	$(C_7H_{10}N)_2ZnI_4{\cdot}H_2O$	4.10[3]	3.60	3.36	4.06	4.55
$(BAPMA)Cu_2Br_5$	$(C_7H_{22}N_3)Cu_2Br_5$	2.85[32]	2.25	2.23	2.65	3.59
$(C_7H_8N_3)_2SbBr_5$	$(C_7H_8N_3)_2SbBr_5$	2.79[33]	2.97	2.81	3.26	3.85
$(C_7H_8N_3)_3InBr_6{\cdot}H_2O$	$(C_7H_8N_3)_3InBr_6{\cdot}H_2O$	3.65[33]	2.58	2.58	3.05	3.60
$(C_7H_8N_3)_3InCl_6{\cdot}H_2O$	$(C_7H_8N_3)_3InCl_6{\cdot}H_2O$	4.01[33]	2.92	2.91	3.27	4.08
$(MXD)_2PbI_6$	$(C_8H_{14}N_2)_2PbI_6$	2.33[34]	2.97	2.70	3.31	3.72
$(MXD)_2SnBr_6$	$(C_8H_{14}N_2)_2SnBr_6$	3.00[35]	2.92	2.88	2.98	3.57
$(MXD)_3Bi_2Br_{12}{\cdot}2H_2O$	$(C_8H_{14}N_2)_3Bi_2Br_{12}{\cdot}2H_2O$	2.86[34]	3.32	2.62	3.70	4.39
$(MXD)BiI_5$	$(C_8H_{14}N_2)BiI_5$	2.15[34]	2.69	1.96	3.06	3.55
$(C_8H_{18}N)_2CdCl_4$	$(C_8H_{18}N)_2CdCl_4$	5.52[36]	4.60	4.59	5.21	6.45
$(DCDA)_3Sb_2Cl_{12}$	$(C_8H_{20}N_2)_3Sb_2Cl_{12}$	3.54[37]	3.87	3.59	4.17	4.94
$(PTMA)_2ZnBr_4$	$(C_9H_{14}N)_2ZnBr_4$	4.27[38]	4.01	4.00	4.27	5.19
$(PTMA)_3Cu_3I_6$	$(C_9H_{14}N)_3Cu_3I_6$	3.47[39]	2.23	2.17	2.67	2.57
$(C_9H_{15}N_3)_2SnBr_8$	$(C_9H_{15}N_3)_2SnBr_8$	2.60[40]	1.76	1.75	1.90	2.44
$(C_9NH_{20})_2SbCl_5$	$(C_9NH_{20})_2SbCl_5$	2.88[22]	3.33	3.25	3.69	4.34
$(C_9NH_{20})_2SnBr_4$	$(C_9NH_{20})_2SnBr_4$	2.64[41]	3.53	3.44	4.01	4.90
$(MA)_4InCl_7$	$(CH_3NH_3)_4InCl_7$	3.34[42]	3.96	3.95	4.72	5.38
$\alpha\text{-}Gua_3Cu_2I_5$	$(CH_6N_3)Cu_2I_5$	2.80[43]	2.61	2.58	3.12	3.97

Table S2. The band gap of experimental, GGA, GGA+SOC, R2SCAN, and TASK for 1D OMHHs.

Conventional name	Chemical formula	E_{Exp} (eV)	E_{GGA} (eV)	E_{GGA}^{SOC} (eV)	E_{R2SCAN} (eV)	E_{TASK} (eV)
$BpbmAPb_2I_6$	$C_{22}H_{42}I_6N_2O_4Pb_2S_4$	2.94[44]	2.77	2.56	3.11	3.44
$(H_2NDIEA)Pb_2I_6{\cdot}2DMF$	$C_{12}H_{16}I_3N_3O_3Pb$	1.72[45]	0.52	0.33	0.44	0.88
$(H_2BPP)Pb_2Br_6$	$C_{13}H_{16}N_2Pb_2Br_6$	3.30[46]	2.21	2.13	2.57	2.94
$(H_2BPP)Pb_2Cl_6$	$C_{13}H_{16}N_2Pb_2Cl_6$	3.55[46]	2.38	2.36	2.96	3.17
$[(Me)_2$-DABCO$]_2Ag_5Pb_2I_{13}$	$C_{16}N_4H_{36}Ag_5Pb_2I_{13}$	2.33[47]	2.70	2.20	2.94	3.90
$[(Me)_2$-DABCO$]_2Cu_5Pb_2I_{13}$	$C_{16}N_4H_{36}Cu_5Pb_2I_{13}$	2.34[47]	2.03	1.59	2.36	2.82
$(HDABCO)_3Ag_5Cl_8$	$C_{18}H_{39}N_6Ag_5Cl_8$	3.05[48]	2.59	2.56	3.01	4.04
$(DTHPE)_{0.5}PbCl_3$	$C_{2.5}H_5NPbCl_3$	3.83[49]	3.85	3.54	4.23	4.95
$PDACuI_3$	$C_3N_2H_{12}CuI_3$	4.03[50]	2.45	2.39	3.09	3.85
$C_4N_2H_{14}PbCl_4$	$C_4N_2H_{14}PbCl_4$	3.58[51]	3.29	2.86	3.64	4.82
$[(H_2NDIEA)_2Pb_5I_{14}{\cdot}(DMF)_2]{\cdot}4DMF$	$C_{54}H_{78}I_{14}N_{14}Pb_5$	1.70[45]	0.74	0.53	0.97	1.10
$C_5H_{14}N_2PbCl_4{\cdot}H_2O$	$C_5H_{14}N_2PbCl_4{\cdot}H_2O$	3.53[52]	2.54	1.81	3.05	4.18
$[DMTHP]PbCl_3$	$C_6H_{12}N_2PbCl_3$	3.77[49]	3.69	3.51	4.17	4.68
$[H_2DABCO][Ag_2Br_4(DABCO)]$	$C_6H_{13}N_2AgBr_2$	3.44[48]	2.62	2.61	3.35	4.16
$[H_2DABCO][Ag_2I_4(DABCO)]$	$C_6H_{13}N_2AgI_2$	2.84[48]	2.89	2.72	3.18	4.46
$[H_2DABCO]Cu_3Br_5$	$C_6N_2H_{14}Cu_3Br_5$	3.44[53]	1.61	1.60	2.00	2.94
$[H_2DABCO]Cu_3I_5$	$C_6N_2H_{14}Cu_3I_5$	3.20[53]	1.92	1.86	2.40	3.25
$[DBN]PbCl_3$	$C_7H_{13}N_2PbCl_3$	3.53[49]	4.13	3.56	4.43	5.32
[*N*-methyldabconium]PbI_3	$C_7H_{15}N_2PbI_3$	2.92[54]	3.40	2.67	3.69	4.67
$[Me\text{-}MePy]Cu_2I_3$	$C_7NH_{10}Cu_2I_3$	2.85[53]	0.87	0.74	1.27	1.04
$[(Me)_2$-DABCO$]Ag_2PbBr_6$	$C_8N_2H_{18}Ag_2PbBr_6$	2.77[47]	3.07	2.65	3.49	4.43
$[(Me)_2$-DABCO$]Cu_2I_4$	$C_8N_2H_{18}Cu_2I_4$	3.27[53]	2.28	2.24	2.72	3.16
CEPbBr	$(ClCH_2CH_2N(CH_3)_3)PbBr_3$	3.33[55]	3.77	3.16	4.15	5.27
$NH_3(CH_3)_6NH_3BiI_5$	$(C_6H_{13}N)_2BiI_5$	2.05[56]	2.20	1.56	2.31	2.99
R-3-ADP-$SbBr_5$	$C_5H_{14}Br_5N_2Sb$	2.47[57]	2.51	2.28	2.71	3.30
R-3-HP-$PbBr_3$	R-$C_5H_{11}NOPbBr_3$	3.29[58]	3.75	3.14	4.05	5.24
S-2-$MPDPbBr_3$	S-$C_6H_{13}HPbBr_3$	3.51[59]	3.86	3.25	4.19	5.42
S-2-$MPDPbI_3$	S-$C_6H_{13}HPbI_3$	2.53[59]	3.38	2.62	3.67	4.72
S-$MBABiI_4$	S-$C_8H_{11}BiI_4N$	1.77[60]	2.69	1.80	2.88	3.53
S-$MBASbI_4$	S-$C_8H_{11}SbI_4N$	2.56[61]	2.37	2.04	2.43	3.01
$TMEDAPb_2Br_6$	$C_5H_{16}N_2Pb_2Br_6$	3.10[62]	3.33	2.84	3.69	4.82
$(2,4,6\text{-}TMP)PbBr_3$	$(C_8H_{11}N)PbBr_3$	3.47[63]	2.67	2.60	3.06	3.46

(2,6-LD)$PbBr_3$	$((CH_3)_2C_5H_3N)PbBr_3$	3.6[63]	2.23	2.17	2.51	3.01
(2-PP)$PbBr_3$	$(C_{11}H_9N)PbBr_3$	3.44[63]	2.20	2.12	2.45	2.90
$(2Sprm)_2InCl_5$	$(C_4H_5N_2S)_2InCl_5$	2.58[64]	2.15	2.14	2.46	2.83
(2cepiH)$CdCl_3$	$(C_7H_{15}ClN)CdCl_3$	3.35[65]	4.27	4.27	5.11	6.05
(2cepyH)PbI_3	$(C_6H_{13}Cl_2N)PbI_3$	2.75[66]	3.27	2.61	3.51	4.56
(4-PP)$PbBr_3$	$(C_{11}H_9N)PbBr_3$	3.42[63]	2.29	2.22	2.65	3.00
$(Bpeb)_2CdCl_4$	$(C_{20}H_{16}N_2)CdCl_4$	2.16[67]	1.68	1.68	1.72	2.08
$(Bpeb)_2Pb_3Cl_6$	$(C_{20}H_{16}N_2)Pb_3Cl_6$	1.91[67]	1.51	1.51	1.44	1.91
$(Bpeb)_2ZnCl_4$	$(C_{20}H_{16}N_2)ZnCl_4$	2.12[67]	1.66	1.67	1.71	2.07
$(C_{12}H_{24}O_6)CsCu_2Br_3$	$(C_{12}H_{24}O_6)CsCu_2Br_3$	1.85[68]	2.19	2.17	2.58	2.97
$(C_3H_7NO)_2SbBr_5$	$(C_3H_7NO)_2SbBr_5$	2.75[69]	2.57	2.39	2.72	3.36
$(C_3H_7NO)_2SbCl_5$	$(C_3H_7NO)_2SbCl_5$	3.21[69]	3.07	2.87	3.16	3.99
$(C_4H_{10}NO)_2SbCl_5$	$(C_4H_{10}NO)_2SbCl_5$	3.25[70]	3.39	3.17	3.61	4.50
$TMGPbI_3$	$(C_5H_{13}N_3)PbI_3$	3.07[71]	3.43	2.68	3.57	4.73
$(2,6\text{-}dmpz)_3Pb_2Br_{10}$	$(C_6H_{16}N_2)_3Pb_2Br_{11}$	3.16[72]	3.11	2.41	3.14	4.15
$(C_6H_{18}N_2O_2)PbBr_4$	$(C_6H_{18}N_2O_2)PbBr_4$	3.79[73]	2.66	2.18	2.92	4.07
(hep)$PbBr_3$	$(C_7H_{16}N)PbBr_4$	3.10[72]	3.53	3.02	3.88	5.04
$(C_8H_9N_2)MnCl_3{\cdot}2H_2O$	$(C_8H_9N_2)MnCl_3{\cdot}2H_2O$	4.37[74]	3.02	3.03	3.40	4.01
$(C_9H_{14}N)SbCl_4$	$(C_9H_{14}N)SbCl_4$	3.47[75]	3.68	3.56	4.05	4.80
(CMP)$CdCl_3$	$(C_6H_7ClN)CdCl_3$	4.09[76]	2.88	2.87	3.44	3.69
(Dipa)PbI_3	$((CH_3)_2CH)_2NH_2PbI_3$	2.64[77]	3.28	2.60	3.59	4.56
$(R\text{-}MPA)_2CdCl_5$	$(R\text{-}C_{10}H_{15}N)_2CdCl_4$	4.42[78]	3.95	3.95	4.12	5.25

References:

(1) Zhang, S.; Zhao, Y.; Zhou, J.; Ming, H.; Wang, C.-H.; Jing, X.; Ye, S.; Zhang, Q. Structural design enables highly-efficient green emission with preferable blue light excitation from zero-dimensional manganese (II) hybrids. *Chemical Engineering Journal* **2021**, *421*, 129886.

(2) Xu, T.; Li, Y.; Nikl, M.; Kucerkova, R.; Zhou, Z.; Chen, J.; Sun, Y.-Y.; Niu, G.; Tang, J.; Wang, Q. Lead-free zero-dimensional organic-copper (I) halides as stable and sensitive X-ray scintillators. *ACS Applied Materials & Interfaces* **2022**, *14* (12), 14157-14164.

(3) He, S.; Hao, S.; Fan, L.; Liu, K.; Cai, C.; Wolverton, C.; Zhao, J.; Liu, Q. Efficient Solar Spectrum-Like White-Light Emission in Zinc-Based Zero-Dimensional Hybrid Metal Halides. *Advanced Optical Materials* **2023**, *11* (15), 2300218.

(4) Zhang, Z.; Liao, J.-F.; Xing, G. Regulating the coordination geometry of polyhedra in zero-dimensional metal halides for tunable emission. *Nanoscale* **2023**, *15* (11), 5241-5248.

(5) Fan, L.; Hao, S.; He, S.; Zhang, X.; Li, M.; Wolverton, C.; Zhao, J.; Liu, Q. Luminescent hybrid halides with various centering metal cations (Zn, Cd and Pb) and diverse structures. *Dalton Transactions* **2023**, *52* (16), 5119-5126.

(6) Liu, X.; Li, Y.; Liang, T.; Fan, J. Role of Polyhedron Unit in Distinct Photophysics of Zero-Dimensional Organic–Inorganic Hybrid Tin Halide Compounds. *The Journal of Physical Chemistry Letters* **2021**, *12* (24), 5765-5773.

(7) Creason, T. D.; Fattal, H.; Gilley, I. W.; Evans, B. N.; Jiang, J.; Pachter, R.; Glatzhofer, D. T.; Saparov, B. Stabilized photoemission from organic molecules in zero-dimensional hybrid Zn and Cd halides. *Inorganic Chemistry Frontiers* **2022**, *9* (23), 6202-6210.

(8) Su, B.; Jin, J.; Peng, Y.; Molokeev, M. S.; Yang, X.; Xia, Z. Zero-Dimensional Organic Copper (I) Iodide Hybrid with High Anti-Water Stability for Blue-Light-Excitable Solid-State Lighting. *Advanced Optical Materials* **2022**, *10* (12), 2102619.

(9) Li, K.-J.; Zhao, Y.-Y.; Sun, M.-E.; Chen, G.-S.; Zhang, C.; Liu, H.-L.; Li, H.-Y.; Zang, S.-Q.; Mak, T. C. Zero-dimensional zinc halide organic hybrids with excellent optical waveguide properties. *Crystal Growth & Design* **2022**, *22* (5), 3295-3302.

(10) Liu, F.; Mondal, D.; Zhang, K.; Zhang, Y.; Huang, K.; Wang, D.; Yang, W.; Mahadevan, P.; Xie, R. Zero-dimensional plate-shaped copper halide crystals with green-yellow emissions. *Materials Advances* **2021**, *2* (11), 3744-3751.

(11) Peng, H.; Tian, Y.; Yu, Z.; Wang, X.; Ke, B.; Zhao, Y.; Dong, T.; Wang, J.; Zou, B. (C16H28N) 2SbCl5: A new lead-free zero-dimensional metal-halide hybrid with bright orange emission. *Science China Materials* **2022**, *65* (6), 1594-1600.

(12) Peng, H.; Tian, Y.; Zhang, Z.; Wang, X.; Huang, T.; Dong, T.; Xiao, Y.; Wang, J.; Zou, B. Bulk assembly of zero-dimensional organic copper bromide hybrid with bright self-trapped exciton emission and high antiwater stability. *The Journal of Physical Chemistry C* **2021**, *125* (36), 20014-20021.

(13) Lian, L.; Zhang, P.; Liang, G.; Wang, S.; Wang, X.; Wang, Y.; Zhang, X.; Gao, J.; Zhang, D.; Gao, L. Efficient dual-band white-light emission with high color rendering from zero-dimensional organic copper iodide. *ACS applied materials & interfaces* **2021**, *13* (19), 22749-22756.

(14) Peng, Y.-C.; Zhou, S.-H.; Jin, J.-C.; Zhuang, T.-H.; Gong, L.-K.; Lin, H.-W.; Wang, Z.-P.; Du, K.-Z.; Huang, X.-Y. [PPh3H] 2 [SbCl5]: a zero-dimensional hybrid metal halide with a supramolecular framework and stable dual-band emission. *The Journal of Physical Chemistry C* **2022**, *126* (40), 17381-17389.
(15) Li, B.; Jin, J.; Yin, M.; Zhang, X.; Molokeev, M. S.; Xia, Z.; Xu, Y. Sequential and Reversible Phase Transformations in Zero-Dimensional Organic-Inorganic Hybrid Sb-based Halides towards Multiple Emissions. *Angewandte Chemie International Edition* **2022**, *61* (49), e202212741.
(16) Li, B.; Xu, Y.; Zhang, X.; Han, K.; Jin, J.; Xia, Z. Zero-dimensional luminescent metal halide hybrids enabling bulk transparent medium as large-area X-ray scintillators. *Advanced Optical Materials* **2022**, *10* (10), 2102793.
(17) Liu, S.; Fang, X.; Lu, B.; Yan, D. Wide range zero-thermal-quenching ultralong phosphorescence from zero-dimensional metal halide hybrids. *Nature Communications* **2020**, *11* (1), 4649.
(18) Xu, L. J.; Plaviak, A.; Lin, X.; Worku, M.; He, Q.; Chaaban, M.; Kim, B. J.; Ma, B. Metal Halide Regulated Photophysical Tuning of Zero-Dimensional Organic Metal Halide Hybrids: From Efficient Phosphorescence to Ultralong Afterglow. *Angewandte Chemie* **2020**, *132* (51), 23267-23271.
(19) Xu, L.-J.; Lin, X.; He, Q.; Worku, M.; Ma, B. Highly efficient eco-friendly X-ray scintillators based on an organic manganese halide. *Nature communications* **2020**, *11* (1), 4329.
(20) Li, M.; Lin, J.; Liu, K.; Fan, L.; Wang, N.; Guo, Z.; Yuan, W.; Zhao, J.; Liu, Q. Light-emitting 0D hybrid metal halide (C3H12N2) 2Sb2Cl10 with antimony dimers. *Inorganic Chemistry* **2021**, *60* (15), 11429-11434.
(21) Teri, G.; Ni, H.-F.; Luo, Q.-F.; Wang, X.-P.; Wang, J.-Q.; Fu, D.-W.; Guo, Q. Tin-based organic–inorganic metal halides with a reversible phase transition and thermochromic response. *Materials Chemistry Frontiers* **2023**, *7* (11), 2235-2240.
(22) Zhou, C.; Lin, H.; Tian, Y.; Yuan, Z.; Clark, R.; Chen, B.; van de Burgt, L. J.; Wang, J. C.; Zhou, Y.; Hanson, K. Luminescent zero-dimensional organic metal halide hybrids with near-unity quantum efficiency. *Chemical science* **2018**, *9* (3), 586-593.
(23) Jiang, X.; Chen, Z.; Tao, X. (1-C5H14N2Br) 2MnBr 4: A Lead-Free Zero-Dimensional Organic-Metal Halide With Intense Green Photoluminescence. *Frontiers in Chemistry* **2020**, *8*, 352.
(24) Li, D.-Y.; Liu, Y.-H.; Wang, Q.; Lei, X.-W.; Yue, C.-Y.; Jing, Z.-H. Zero-dimensional hybrid zinc halides with blue light emissions. *Materials Today Chemistry* **2023**, *31*, 101604.
(25) Wang, Y.; Zhang, S.; Wang, Y.; Yan, J.; Yao, X.; Xu, M.; Lei, X.-w.; Lin, G.; Yue, C.-y. 0D triiodide hybrid halide perovskite for X-ray detection. *Chemical Communications* **2023**, *59* (60), 9239-9242.
(26) Zhu, S.; Pan, J.; Chen, X.; Chen, H.; Pan, S. Solution growth and optical properties of lead-free highly efficient green-emitting [Emim] 4 [Cu4I8] single crystals with 0D structure. *Journal of Luminescence* **2023**, *253*, 119467.
(27) Gao, H.; Lu, Z.; Zhao, X.; Zhang, K.; Zhu, X.; Cheng, R.; Li, S.-L.; Qi, Z.; Zhang, X.-M. Singlet exciton and singlet/triplet self-trapped excitons for ultra-broadband white-light

emission in a zero-dimensional cadmium bromide hybrid. *Journal of Materials Chemistry C* **2023**, *11* (26), 9023-9029.
(28) Zhao, J.-Q.; Shi, H.-S.; Zeng, L.-R.; Ge, H.; Hou, Y.-H.; Wu, X.-M.; Yue, C.-Y.; Lei, X.-W. Highly emissive zero-dimensional antimony halide for anti-counterfeiting and confidential information encryption-decryption. *Chemical Engineering Journal* **2022**, *431*, 134336.
(29) Qi, Z.; Gao, H.; Zhu, X.; Lu, Z.; Zhang, X.-M. Blue light-excitable broadband yellow emission in a zero-dimensional hybrid bismuth halide with type-II band alignment. *Inorganic Chemistry* **2022**, *61* (48), 19483-19491.
(30) Wei, X.; He, J.; Zhu, Y.; Qin, Z.; Zheng, G.; Zhang, R.; Mo, S.; Wang, J.; Yao, D.; Lin, B. Synthesis, structure, and photoelectric properties of a novel zero-dimensional organic-inorganic hybrid perovskite (C6H9N2) 2MnI4. *Optical Materials* **2023**, *136*, 113360.
(31) Liu, Y.-H.; Wang, W.-Q.; Zhang, B.-L.; Wang, Y.-J.; Ren, M.-P.; Jing, Z.; Yue, C.-Y. Zero-dimensional organic–inorganic hybrid zinc halide with broadband yellow light emission. *CrystEngComm* **2023**, *25* (3), 444-449.
(32) Liu, Y.-H.; Wang, N.-N.; Ren, M.-P.; Yan, X.; Wu, Y.-F.; Yue, C.-Y.; Lei, X.-W. Zero-dimensional hybrid cuprous halide of [BAPMA] Cu2Br5 as a highly efficient light emitter and an X-ray scintillator. *ACS Applied Materials & Interfaces* **2023**, *15* (16), 20219-20227.
(33) Lin, J.; Liu, K.; Ruan, H.; Sun, N.; Chen, X.; Zhao, J.; Guo, Z.; Liu, Q.; Yuan, W. Zero-dimensional lead-free halide with indirect optical gap and enhanced photoluminescence by Sb doping. *The Journal of Physical Chemistry Letters* **2021**, *13* (1), 198-207.
(34) Klee, P. S.; Hirano, Y.; Cordes, D. B.; Slawin, A. M.; Payne, J. L. Synthesis, Structure, and Tunability of Zero-Dimensional Organic–Inorganic Metal Halides Utilizing the m-Xylylenediammonium Cation: MXD2PbI6, MXDBiI5, and MXD3Bi2Br12· 2H2O. *Crystal Growth & Design* **2022**, *22* (6), 3815-3823.
(35) Su, B.; Song, G.; Molokeev, M. S.; Lin, Z.; Xia, Z. Synthesis, crystal structure and green luminescence in zero-dimensional tin halide (C8H14N2) 2SnBr6. *Inorganic Chemistry* **2020**, *59* (14), 9962-9968.
(36) Wang, D.-L.; Sun, D.-F.; Xu, L.-Y.; Liu, J.; Wang, J.-Y.; Shen, C.-Y. The synthesis, structure and photoluminescence of new (C8H18N) 2CdCl4 crystals. *Journal of Molecular Structure* **2023**, *1282*, 135222.
(37) Chai, C.-Y.; Han, X.-B.; Liu, C.-D.; Fan, C.-C.; Liang, B.-D.; Zhang, W. Circularly polarized luminescence in zero-dimensional antimony halides: structural distortion controlled luminescence thermometer. *The Journal of Physical Chemistry Letters* **2023**, *14* (17), 4063-4070.
(38) Chen, Q.; Dai, F.; Zhang, K.; Zhou, H.; Zhang, M.; Quan, D.; Wang, L.; Xing, J. Synthesis, crystal structure and white luminescence of zero-dimensional organic–inorganic zinc halides. *Journal of Materials Chemistry C* **2022**, *10* (48), 18279-18284.
(39) Lian, L.; Zhang, T.; Ding, H.; Zhang, P.; Zhang, X.; Zhao, Y.-B.; Gao, J.; Zhang, D.; Zhao, Y. S.; Zhang, J. Highly luminescent zero-dimensional organic copper halide with low-loss optical waveguides and highly polarized emission. *ACS Materials Letters* **2022**, *4* (8), 1446-1452.
(40) Liu, K.; Hao, S.; Cao, J.; Lin, J.; Fan, L.; Zhang, X.; Guo, Z.; Wolverton, C.; Zhao, J.; Liu, Q. Antimony doping to enhance luminescence of tin (IV)-based hybrid metal halides. *Inorganic Chemistry Frontiers* **2022**, *9* (15), 3865-3873.

(41) Zhou, C.; Lin, H.; Shi, H.; Tian, Y.; Pak, C.; Shatruk, M.; Zhou, Y.; Djurovich, P.; Du, M. H.; Ma, B. A zero-dimensional organic seesaw-shaped tin bromide with highly efficient strongly stokes-shifted deep-red emission. *Angewandte Chemie* **2018**, *130* (4), 1033-1036.
(42) Lin, F.; Yu, G.; Weng, S.; Zhou, C.; Han, Y.; Liu, W.; Zhou, K.; Wang, Y.; Lin, H. Blue photoluminescence enhancement achieved by zero-dimensional organic indium halides via a metal ion doping strategy. *Materials Chemistry Frontiers* **2023**, *7* (1), 137-144.
(43) Wu, J.; Guo, Y.; Qi, J. L.; Yao, W. D.; Yu, S. X.; Liu, W.; Guo, S. P. Multi-Stimuli Responsive Luminescence and Domino Phase Transition of Hybrid Copper Halides with Nonlinear Optical Switching Behavior. *Angewandte Chemie* **2023**, *135* (18), e202301937.
(44) Febriansyah, B.; Koh, T. M.; John, R. A.; Ganguly, R.; Li, Y.; Bruno, A.; Mhaisalkar, S. G.; England, J. Inducing panchromatic absorption and photoconductivity in polycrystalline molecular 1D lead-iodide perovskites through π-stacked viologens. *Chemistry of Materials* **2018**, *30* (17), 5827-5830.
(45) Fang, H.; Chen, F.-H.; Zhang, S.-Q.; Lin, M.-J. Three semiconductive 1D naphthalene diimide/iodoplumbate perovskites with high moisture tolerance and long-lived charge separation states. *Inorganic Chemistry* **2023**, *62* (24), 9661-9670.
(46) Sun, X.-Y.; Yue, M.; Jiang, Y.-X.; Zhao, C.-H.; Liao, Y.-Y.; Lei, X.-W.; Yue, C.-Y. Combining dual-light emissions to achieve efficient broadband yellowish-green luminescence in one-dimensional hybrid lead halides. *Inorganic Chemistry* **2021**, *60* (3), 1491-1498.
(47) Yue, C.-Y.; Sun, C.; Li, D.-Y.; Dong, Y.-H.; Wang, C.-L.; Zhao, H.-F.; Jiang, H.; Jing, Z.-H.; Lei, X.-W. Organic–Inorganic Hybrid Heterometallic Halides with Low-Dimensional Structures and Red Photoluminescence Emissions. *Inorganic Chemistry* **2019**, *58* (15), 10304-10312.
(48) Sun, C.; Guo, Y.-H.; Yuan, Y.; Chu, W.-X.; He, W.-L.; Che, H.-X.; Jing, Z.-H.; Yue, C.-Y.; Lei, X.-W. Broadband White-Light Emission in One-Dimensional Organic–Inorganic Hybrid Silver Halide. *Inorganic Chemistry* **2020**, *59* (7), 4311-4319.
(49) Zhang, W.-F.; Pan, W.-J.; Xu, T.; Song, R.-Y.; Zhao, Y.-Y.; Yue, C.-Y.; Lei, X.-W. One-dimensional face-shared perovskites with broad-band bluish white-light emissions. *Inorganic Chemistry* **2020**, *59* (19), 14085-14092.
(50) Du, Y.; Ma, L.; Yan, Z.; Xiao, J.; Wang, K.; Lin, T.; Han, X.; Xia, D. One-dimensional hybrid copper (I) iodide single crystal with renewable scintillation properties. *Inorganic Chemistry* **2023**, *62* (29), 11350-11359.
(51) Wu, G.; Zhou, C.; Ming, W.; Han, D.; Chen, S.; Yang, D.; Besara, T.; Neu, J.; Siegrist, T.; Du, M.-H. A one-dimensional organic lead chloride hybrid with excitation-dependent broadband emissions. *ACS Energy Letters* **2018**, *3* (6), 1443-1449.
(52) Peng, Y.; Yao, Y.; Li, L.; Wu, Z.; Wang, S.; Luo, J. White-light emission in a chiral one-dimensional organic–inorganic hybrid perovskite. *Journal of Materials Chemistry C* **2018**, *6* (22), 6033-6037.
(53) Yue, C.-Y.; Lin, N.; Gao, L.; Jin, Y.-X.; Liu, Z.-Y.; Cao, Y.-Y.; Han, S.-S.; Lian, X.-K.; Hu, B.; Lei, X.-W. Organic cation directed one-dimensional cuprous halide compounds: syntheses, crystal structures and photoluminescence properties. *Dalton Transactions* **2019**, *48* (27), 10151-10159.

(54) Xue, C.; Yao, Z.-Y.; Zhang, J.; Liu, W.-L.; Liu, J.-L.; Ren, X.-M. Extra thermo-and water-stable one-dimensional organic–inorganic hybrid perovskite [N-methyldabconium] PbI 3 showing switchable dielectric behaviour, conductivity and bright yellow-green emission. *Chemical Communications* **2018**, *54* (34), 4321-4324.
(55) Li, D.-F.; Zhao, P.-J.; Deng, X.-H.; Wu, Y.-Z.; He, X.-L.; Liu, D.-S.; Li, Y.-X.; Sui, Y. A new organic–inorganic hybrid perovskite ferroelectric [ClCH 2 CH 2 N (CH 3) 3][PbBr 3] and Its PVDF matrix-assisted highly-oriented flexible ferroelectric films. *New Journal of Chemistry* **2022**, *46* (40), 19391-19400.
(56) Zhang, W.; Tao, K.; Ji, C.; Sun, Z.; Han, S.; Zhang, J.; Wu, Z.; Luo, J. (C6H13N) 2BiI5: a one-dimensional lead-free perovskite-derivative photoconductive light absorber. *Inorganic chemistry* **2018**, *57* (8), 4239-4243.
(57) Qi, S.; Cheng, P.; Han, X.; Ge, F.; Shi, R.; Xu, L.; Li, G.; Xu, J. Organic–inorganic hybrid antimony (III) halides for second harmonic generation. *Crystal Growth & Design* **2022**, *22* (11), 6545-6553.
(58) Peng, X. L.; Han, R. R.; Tang, Y. Z.; Tan, Y. H.; Fan, X. W.; Wang, F. X.; Zhang, H. 1D Chiral Lead Bromide Perovskite with Superior Second-Order Optical Nonlinearity, Photoluminescence, and High-Temperature Reversible Phase Transition. *Chemistry–An Asian Journal* **2023**, *18* (4), e202201206.
(59) Zheng, Y.; Xu, J.; Bu, X. H. 1D Chiral Lead Halide Perovskites with Superior Second-Order Optical Nonlinearity. *Advanced Optical Materials* **2022**, *10* (1), 2101545.
(60) Yao, L.; Zeng, Z.; Cai, C.; Xu, P.; Gu, H.; Gao, L.; Han, J.; Zhang, X.; Wang, X.; Wang, X. Strong second-and third-harmonic generation in 1D chiral hybrid bismuth halides. *Journal of the American Chemical Society* **2021**, *143* (39), 16095-16104.
(61) Yao, L.; Xue, K.-H.; Tong, H.; Chen, C.; Niu, G.; Yang, W.; Tang, J. Dimensional Control of Chiral Antimony Halide Compounds for Enhanced Circular Dichroism. *Crystal Growth & Design* **2022**, *22* (9), 5552-5558.
(62) Lin, H.; Zhou, C.; Neu, J.; Zhou, Y.; Han, D.; Chen, S.; Worku, M.; Chaaban, M.; Lee, S.; Berkwits, E. Bulk assembly of corrugated 1D metal halides with broadband yellow emission. *Advanced Optical Materials* **2019**, *7* (6), 1801474.
(63) Chen, R.; Sun, C.; Cheng, X.; Lin, Y.; Zhou, J.; Yin, J.; Cui, B.-B.; Mao, L. One-Dimensional Organic–Inorganic Lead Bromide Hybrids with Excitation-Dependent White-Light Emission Templated by Pyridinium Derivatives. *Inorganic Chemistry* **2023**, *62* (24), 9722-9731. DOI: 10.1021/acs.inorgchem.3c00997.
(64) Owczarek, M.; Lee, M.; Zapf, V.; Nie, W.; Jakubas, R. Accessing One-Dimensional Chains of Halogenoindates (III) in Organic–Inorganic Hybrids. *Inorganic Chemistry* **2022**, *61* (14), 5469-5473.
(65) Qi, Z.; Chen, Y.; Guo, Y.; Yang, X.; Zhang, F.-Q.; Zhou, G.; Zhang, X.-M. Broadband white-light emission in a one-dimensional organic–inorganic hybrid cadmium chloride with face-sharing CdCl 6 octahedral chains. *Journal of Materials Chemistry C* **2021**, *9* (1), 88-94.
(66) Qi, Z.; Gao, H.; Yang, X.; Chen, Y.; Zhang, F.-Q.; Qu, M.; Li, S.-L.; Zhang, X.-M. A One-Dimensional Broadband Emissive Hybrid Lead Iodide with Face-Sharing PbI6 Octahedral

Chains. *Inorganic Chemistry* **2021**, *60* (20), 15136-15140. DOI: 10.1021/acs.inorgchem.1c02732.
(67) Wu, S.; Zhou, B.; Yan, D. Low-Dimensional Organic Metal Halide Hybrids with Excitation-Dependent Optical Waveguides from Visible to Near-Infrared Emission. *ACS Applied Materials & Interfaces* **2021**, *13* (22), 26451-26460. DOI: 10.1021/acsami.1c03926.
(68) Huang, J.; Peng, Y.; Jin, J.; Molokeev, M. S.; Yang, X.; Xia, Z. Unveiling White Light Emission of a One-Dimensional Cu(I)-Based Organometallic Halide toward Single-Phase Light-Emitting Diode Applications. *The Journal of Physical Chemistry Letters* **2021**, *12* (51), 12345-12351. DOI: 10.1021/acs.jpclett.1c03767.
(69) Liu, W.-T.; Zhang, Z.-X.; Ding, K.; Fu, D.-W.; Lu, H.-F. Halogen tuning toward dielectric switch and band gap engineering in one-dimensional hybrid materials. *Journal of Molecular Structure* **2022**, *1270*, 133954. DOI: https://doi.org/10.1016/j.molstruc.2022.133954.
(70) Zhuang, J.-C.; Tan, Y.-H.; Fan, X.-W.; Tang, Y.-Z.; Song, N.; Zhang, Y.-H.; Zhang, H.; Chen, S.-P. A 1D chiral infinite chain organic metal halide hybrid with excellent SHG switching and moderate spontaneous polarization. *New Journal of Chemistry* **2022**, *46* (15), 7103-7107, 10.1039/D2NJ00303A. DOI: 10.1039/D2NJ00303A.
(71) Cheng, X.; Yue, S.; Chen, R.; Yin, J.; Cui, B.-B. White Light-Emitting Diodes Based on One-Dimensional Organic–Inorganic Hybrid Metal Chloride with Dual Emission. *Inorganic Chemistry* **2022**, *61* (39), 15475-15483. DOI: 10.1021/acs.inorgchem.2c02085.
(72) Mao, L.; Guo, P.; Kepenekian, M.; Hadar, I.; Katan, C.; Even, J.; Schaller, R. D.; Stoumpos, C. C.; Kanatzidis, M. G. Structural Diversity in White-Light-Emitting Hybrid Lead Bromide Perovskites. *Journal of the American Chemical Society* **2018**, *140* (40), 13078-13088. DOI: 10.1021/jacs.8b08691.
(73) Zhou, G.; Jiang, X.; Molokeev, M.; Lin, Z.; Zhao, J.; Wang, J.; Xia, Z. Optically Modulated Ultra-Broad-Band Warm White Emission in Mn2+-Doped (C6H18N2O2)PbBr4 Hybrid Metal Halide Phosphor. *Chemistry of Materials* **2019**, *31* (15), 5788-5795. DOI: 10.1021/acs.chemmater.9b01864.
(74) Panda, D. P.; Swain, D.; Sarkar, S.; Sundaresan, A. Halogen Bond Induced Structural and Photophysical Properties Modification in Organic–Inorganic Hybrid Manganese Halides. *The Journal of Physical Chemistry Letters* **2023**, *14* (18), 4211-4218. DOI: 10.1021/acs.jpclett.3c00656.
(75) Wu, F.; Wei, Q.; Li, X.; Liu, Y.; Huang, W.; Chen, Q.; Li, B.; Luo, J.; Liu, X. Cooperative Enhancement of Second Harmonic Generation in an Organic–Inorganic Hybrid Antimony Halide. *Crystal Growth & Design* **2022**, *22* (6), 3875-3881. DOI: 10.1021/acs.cgd.2c00257.
(76) Xu, H.; Zhang, Z.; Dong, X.; Huang, L.; Zeng, H.; Lin, Z.; Zou, G. Corrugated 1D Hybrid Metal Halide [C6H7ClN]CdCl3 Exhibiting Broadband White-Light Emission. *Inorganic Chemistry* **2022**, *61* (11), 4752-4759. DOI: 10.1021/acs.inorgchem.2c00169.
(77) Maqbool, S.; Thekkayil, Z.; Mandal, P. 1D Diisopropylammonium Lead Iodide Perovskite Shows Exceptional Optical Stability and Third-Order Nonlinearity. *Advanced Optical Materials* **2023**, *11* (15), 2202942. DOI: https://doi.org/10.1002/adom.202202942.
(78) Li, L.-S.; Tan, Y.-H.; Wei, W.-J.; Gao, H.-Q.; Tang, Y.-Z.; Han, X.-B. Chiral Switchable Low-Dimensional Perovskite Ferroelectrics. *ACS Applied Materials & Interfaces* **2021**, *13* (1), 2044-2051. DOI: 10.1021/acsami.0c19507.